

ON THE ROTATIONAL DYNAMICS OF MAGNETICALLY THREADED DISKS AROUND NEUTRON STARS

M. HAKAN ERKUT¹

*Boğaziçi University, 34342, Bebek, İstanbul, Turkey; Sabancı University, 34956,
Orhanlı-Tuzla, İstanbul, Turkey*

and

M. ALİ ALPAR²

Sabancı University, 34956, Orhanlı-Tuzla, İstanbul, Turkey

ABSTRACT

We investigate the rotational dynamics of disk accretion around a strongly magnetized neutron star with an aligned dipole field. The magnetospheric field is assumed to thread the disk plasma both inside and outside the corotation radius. As a result of disk-star interaction, the magnetic torque on the disk affects the structure of accretion flow to yield the observed spin-up or spin-down rates for a source of given fastness, magnetic field strength, and mass accretion rate. Within the model we obtain a prescription for the dynamical viscosity of such magnetically modified solutions for a Keplerian disk. We then use this prescription to find a model solution for the rotation rate profile throughout the entire disk including the non-Keplerian inner disk. We find that the non-Keplerian angular velocity transition region is not necessarily narrow for a source of given spin state. The boundary layer approximation, as in the standard magnetically threaded disk model, holds only in the case of dynamical viscosity decreasing all the way to the innermost edge of the disk. These results are applied to several observed disk-fed X-ray pulsars that have exhibited quasi-periodic oscillations (QPOs). The QPO frequencies provide a constraint on the fastness parameter and enable one to determine uniquely the width of the angular velocity transition zone for each source within model assumptions. We discuss the implications of these results on the value of the critical fastness parameter for a magnetized star

¹hakane@sabanciuniv.edu

²alpar@sabanciuniv.edu

in spin equilibrium. Applications of our model are also made with relevant parameters from recent numerical simulations of quasi-stationary disk-magnetized star interactions.

Subject headings: accretion, accretion disks — magnetic fields — stars: magnetic fields — stars: neutron — X-rays: stars

1. INTRODUCTION

The evidence for the interaction between a rotating magnetized star and a surrounding accretion disk emerges in a wide variety of astrophysical systems such as X-ray binary pulsars (Joss & Rappaport 1984), magnetic white dwarfs in cataclysmic variables (Warner 1995), and T Tauri stars (Basri & Bertout 1989). The detailed modelling of this interaction would contribute to our understanding of many problems like the time rate of change in the pulse periods of the disk fed neutron stars and the quasi-periodic oscillations (QPOs) observed in some sources (Alpar & Shaham 1985; Aly & Kuijpers 1990).

In the early investigations (Scharlemann 1978; Ghosh & Lamb 1978; Aly 1980), the degree of diamagnetism presumed for the disk plasma has led to very different magnetic field configurations. If the disk is fully diamagnetic, then it excludes the stellar field completely and the accretion flow from the disk midplane to the surface of the star is assumed to start within a very narrow region near the inner disk radius (Ichimaru 1978). If the accreting plasma has a non-zero resistivity, then the stellar field may penetrate the disk and thread it in a broad zone via the Kelvin-Helmholtz instability, magnetic field reconnection with small scale fields in the disk and turbulent diffusion (Ghosh & Lamb 1979, hereafter GL79; Wang 1987, hereafter W87). One of the most important predictions of the magnetically threaded disk (MTD) model is that the star can spin down while matter accretes on it.

In the MTD model of GL79, the star-disk interaction region consists of two distinct parts. In a broad outer transition zone, where the angular velocity is Keplerian, the effective viscous stress is dominant compared to magnetic stress associated with the twisted field lines. The disk matter is brought into corotation with the neutron star only in a narrow inner transition zone or boundary layer within which magnetic stress dominates over viscous stress. The disk resistivity is very high so that the magnetic diffusivity exceeds the turbulent viscosity by several orders of magnitude. The coronal plasma outside the disk is force-free and the disk is threaded over a large range of radii by magnetic field lines that close through the neutron star.

The study of field line twisting in a force-free magnetosphere has revealed that a closed

field line tends to inflate and evolve into an open one breaking the disk-star link (Lynden-Bell & Boily 1994; Lovelace, Romanova, & Bisnovatyi-Kogan 1995, hereafter LRBK95). The strong outflows associated with the opening of magnetic field lines were reported in several two dimensional magnetohydrodynamic (MHD) simulations (Hayashi, Shibata, & Matsumoto 1996; Miller & Stone 1997; Goodson, Winglee, & Böhm 1997; Goodson, Böhm, & Winglee 1999). Although these numerical studies indicated that the accretion flow around a strongly magnetized object can be nonstationary and episodic in character, the recent MHD simulations by Romanova et al. (2002, hereafter RUKL02) showed that quiescent accretion regimes are also possible provided a matter dominated differentially rotating corona instead of a magnetically dominated force-free one is used as an equilibrium initial condition to examine quasi-stationary situations. The main reason for obtaining different results in the above mentioned simulations is that in the case of a corona corotating with the central star (or non-rotating corona), the initial discontinuity in the angular velocity between the Keplerian disk and the magnetosphere leads to huge field twisting on the corona-disk boundary. This gives rise to the generation of very large toroidal field and to strong magnetic braking of the disk. A differentially rotating matter dominated corona is an appropriate initial condition to avoid this discontinuity (Romanova et al. 1998). It reduces the initial magnetic braking of the disk and allows one to investigate the quiescent phase of disk-star interaction in long-term numerical simulations (RUKL02).

The physical mechanism responsible for the disruption of the inner region of an axisymmetric disk around a magnetic rotator was investigated by a number of authors (Brandenburg & Campbell 1998; Campbell & Heptinstall 1998, hereafter CH98). Integrating the relevant MHD equations radially from the weakly magnetic outer disk regions inwards, they found a vertically disrupted and viscously unstable disk solution inside a critical radius. They also argued that the viscous instability associated with the elevated temperature in the inner disk regions is due to magnetically enhanced viscous dissipation, which causes the vertical equilibrium to break down when the radiation pressure becomes significant. We point out in the present paper (see §§ 3 and 4), that the viscous instability proposed by these authors as the mechanism responsible for the truncation of the inner disk is a consequence of choosing Keplerian rotation for the disk plasma throughout the accretion flow, artificial in the sense that the angular motion could easily be modified by the huge viscous stress estimated for the inner parts of the disk.

For a disk around a non-magnetized star, Glatzel (1992) solved this problem without making the assumption that the rotation rate is Keplerian except in a very narrow boundary layer. In this paper we will present the analogous solution for the magnetic case, allowing for non-Keplerian rotation in the inner disk. Numerical simulations by RUKL02 also have shown non-Keplerian rotation in the magnetically braked inner regions of the disk. We consider

an axisymmetric thin disk threaded by the magnetic dipole field of an aligned rotator and explore the effect of the rotating magnetosphere on the angular velocity profile of the disk plasma. In § 2 we introduce the relevant MHD equations to derive a dimensionless function for the vertically integrated dynamical viscosity. In § 3 we discuss the behavior of this function in connection with the net torque acting on the central star. In § 4 we employ the dynamical viscosity and solve the equation of angular momentum conservation for the rotation profile of a disk around a neutron star in spin equilibrium without making boundary layer approximation. We apply our model to several X-ray binary pulsars that have exhibited QPOs. Using the observed periods, X-ray luminosities, QPO frequencies, and spin-up or spin-down rates of these sources, we obtain constraints on the model parameters within the beat frequency model and estimate the appropriate disk rotation curve for each source. We find that the inner disk rotation rate adapts to Keplerian rotation in the outer disk through a transition zone whose width and rotation rate profile are such as to accommodate the mass accretion rate, rotation period, and magnetic moment of the central object and to yield the observed spin-up or spin-down rates. In § 5 we concentrate on the qualitative similarities between our model and the results of numerical simulations by RUKL02 on the disk structure. Using their numerical data, we roughly estimate the radius where the disk structure is significantly changed and magnetic braking is efficient. We summarize and discuss our results in § 6.

2. BASIC EQUATIONS

The steady-state equation of conservation of angular momentum for an axisymmetric magnetized disk around a neutron star having a dipole moment aligned with its rotation axis can be written in cylindrical coordinates (r, ϕ, z) as

$$\begin{aligned}
 r\rho v_r \frac{\partial}{\partial r} (rv_\phi) + r\rho v_z \frac{\partial}{\partial z} (rv_\phi) &= \frac{\partial}{\partial r} \left[\nu \rho r^3 \frac{\partial}{\partial r} \left(\frac{v_\phi}{r} \right) \right] \\
 &+ \frac{rB_r}{4\pi} \frac{\partial}{\partial r} (rB_\phi) \\
 &+ \frac{r^2 B_z}{4\pi} \frac{\partial B_\phi}{\partial z}, \tag{1}
 \end{aligned}$$

where ν is the coefficient of viscosity. The conservation of mass for a steady-state, axisymmetric disk is given by the continuity equation,

$$\frac{\partial}{\partial r} (r\rho v_r) + \frac{\partial}{\partial z} (r\rho v_z) = 0, \tag{2}$$

which can be vertically integrated to yield the constant mass influx condition,

$$-2\pi \int_{-H}^H r \rho v_r dz = \dot{M} , \quad (3)$$

provided that ρv_z is negligible at $z = \pm H$, a valid assumption except for the case of strong winds or magnetically driven outflows. Here, \dot{M} is the constant mass inflow rate and H is the half-thickness of the disk.

In a geometrically thin accretion disk (i.e., $H \ll r$), the angular momentum balance (1) can be approximated as

$$\begin{aligned} \frac{\partial}{\partial r} (r \rho v_r r^2 \Omega) + \frac{\partial}{\partial z} (r \rho v_z r^2 \Omega) &= \frac{\partial}{\partial r} \left(\nu \rho r^3 \frac{\partial \Omega}{\partial r} \right) \\ &+ \frac{r^2 B_z}{4\pi} \frac{\partial B_\phi}{\partial z} , \end{aligned} \quad (4)$$

where $v_\phi = \Omega r$ is used and the $r\phi$ component of the magnetic stress is neglected in comparison with the last term in equation (1), for the ratio of their magnitudes in the thin disk limit gives

$$\frac{|r B_r \partial_r (r B_\phi)|}{|r^2 B_z \partial_z B_\phi|} \sim \left| \frac{B_r}{B_z} \right| \left(\frac{H}{r} \right) \ll 1 , \quad (5)$$

provided $|B_r/B_z| \ll r/H$, a condition that can only be violated for extremely large disk conductivities.

The vertically averaged form of the angular momentum equation (4), together with the use of equation (3), is finally obtained as

$$\frac{d}{dr} \left(2\pi \nu \Sigma r^3 \frac{d\Omega}{dr} + \dot{M} r^2 \Omega \right) = -r^2 B_z B_\phi^+ , \quad (6)$$

where $B_\phi^+(r) \equiv B_\phi(r, z = H) = -B_\phi(r, z = -H)$ due to the field antisymmetry and Σ is the surface density function defined by

$$\Sigma(r) = \int_{-H}^H \rho(r, z) dz = 2\rho H , \quad (7)$$

where ρ denotes simply the vertically averaged density. The last term in equation (1) was also identified as the dominant magnetic term in the early derivation of equation (6) by Campbell (1992) for steady disks and by Lovelace, Romanova, & Newman (1994) in a form appropriate for time-dependent disks with outbursts.

The vertical component of the magnetic field threading the disk can be expressed, in general, as

$$B_z(r) = -s(r) \mu_* r^{-3} , \quad (8)$$

where $\mu_* = (1/2) B_* R_*^3$ is the dipole moment of the neutron star of radius R_* in terms of its polar surface field strength B_* and $s(r)$ represents a screening coefficient which accounts for the effect of induced currents on the pure stellar dipole field in a partially diamagnetic disk. In a self-consistent treatment, the radial dependence of s must be properly found from a detailed analysis of the magnetospheric current system in the corona. The modelling of such a disk-corona-star system is beyond the scope of the present study. In this work, we will rather assume that the vertical component of the magnetic field threading the disk can be represented by

$$B_z(r) = -s_{\text{eff}} \frac{\mu_*}{r^3}, \quad (9)$$

where s_{eff} is an effective screening coefficient taken to be a constant over a wide range of radii (Wang 1995).

The azimuthal component of the magnetic field at the surface of a disk in vertical hydrostatic equilibrium (i.e., $v_z = 0$) can be estimated from the toroidal component of the induction equation, which can be written under the assumptions of steady-state and axisymmetry as

$$\begin{aligned} \frac{\partial}{\partial z} (\Omega r B_z) + \frac{\partial}{\partial r} (\Omega r B_r) - \frac{\partial}{\partial r} (v_r B_\phi) \\ + \frac{\partial}{\partial r} \left(\eta \frac{\partial B_\phi}{\partial r} \right) + \frac{\partial}{\partial z} \left(\eta \frac{\partial B_\phi}{\partial z} \right) = 0, \end{aligned} \quad (10)$$

where η is the magnetic diffusivity of the disk. Assuming that all quantities change on a length scale r in the radial direction and H in the vertical direction, the significance of the second term compared with the first term in equation (10) can be estimated as

$$\frac{|\partial_r (\Omega r B_r)|}{|\partial_z (\Omega r B_z)|} \sim \left| \frac{B_r}{B_z} \right| \left(\frac{H}{r} \right) \ll 1, \quad (11)$$

provided we have $|B_r| \lesssim |B_z|$. The last term in equation (10) dominates over the fourth and third terms:

$$\frac{|\partial_r (\eta \partial_r B_\phi)|}{|\partial_z (\eta \partial_z B_\phi)|} \sim \left(\frac{H}{r} \right)^2 \ll 1 \quad (12)$$

and

$$\frac{|\partial_r (v_r B_\phi)|}{|\partial_z (\eta \partial_z B_\phi)|} \sim \frac{|v_r| H}{\eta} \left(\frac{H}{r} \right) \ll 1, \quad (13)$$

provided $\eta \gtrsim |v_r| H$ is satisfied. The consistency of equation (11) with equation (13) can be justified using the poloidal component of the induction equation which can be written as

$$\frac{\partial B_r}{\partial z} - \frac{\partial B_z}{\partial r} + \frac{v_r B_z}{\eta} = 0, \quad (14)$$

where the disk is assumed to be in vertical hydrostatic equilibrium, i.e., $v_z = 0$. For very small radial inflow velocities, i.e., $v_r \ll \eta/r$, equation (14) yields $|B_r| \sim (H/r)|B_z|$ and the distortion of the external field due to accretion becomes negligible. In this case the estimates in equations (11) and (12) are both $O((H/r)^2) \ll 1$, while the estimate in (13) is smaller than $O((H/r)^2)$ by the factor $v_r r/\eta$. If, on the other hand, $|B_r| \lesssim |B_z|$, as is likely when the field is distorted, then $|\partial_r B_z| \ll |\partial_z B_r|$ and we obtain

$$B_r^+ = -\frac{v_r H}{\eta} B_z \quad (15)$$

from the vertical integration of equation (14), where $B_r^+(r) \equiv B_r(r, z = H) = -B_r(r, z = -H)$ following the field antisymmetry (see Lovelace, Romanova, & Newman 1994; also LRBK95). When equation (15) holds, approximations (11) and (13) are both $\lesssim O(H/r) \ll 1$.

Taking the conditions (11), (12), and (13) to be satisfied, the toroidal component of the induction equation (10) can be safely reduced to

$$r B_z \frac{\partial \Omega}{\partial z} + \frac{\partial}{\partial z} \left(\eta \frac{\partial B_\phi}{\partial z} \right) = 0. \quad (16)$$

The vertical gradient of angular velocity depends on the scale height over which the plasma is brought into corotation with the neutron star. In the case of a force-free magnetosphere outside the disk, this scale height can be estimated as H , the half-thickness of the disk, since the magnetic energy density becomes much greater than the kinetic energy density of the plasma for $|z| \geq H$. The resulting twisting of field loops due to this huge vertical shear gradient may lead to an open field line configuration unless $|\partial \Omega / \partial z| < |\Omega_* - \Omega| / H$. The recent time-dependent simulations by RUKL02 have shown that the field line opening is strongly suppressed for a relatively dense corona outside the disk. Assuming that the vertical shear along a flux tube linking the star and the disk is reduced by the inertial effect of a corona, the integration of equation (16) over z can be approximated as

$$B_\phi^+ = \epsilon r (\Omega_* - \Omega) H \eta^{-1} B_z, \quad (17)$$

where the transition from the angular velocity of the disk plasma, Ω , to the rotational rate of the neutron star, Ω_* , takes place within an effective scale height of $\epsilon^{-1}H$ with $\epsilon < 1$ (see Campbell 1992; also LRBK95 for other derivations of eq. [17]). Here, ϵ is a shear reduction factor which may arise from a differentially rotating corona to result in a small field twist at the surface of the disk. Even if the corona is nearly force-free, it cannot be current-free. As the magnetic torque is transmitted to the neutron star by the poloidal currents flowing across the disk surface through the magnetosphere, the rigid-body rotation of the corona may not be realized (see W87; also CH98 for a similar shear reduction factor).

We consider a specific disk region (e.g., a narrow boundary layer of width $\delta r \lesssim H \ll r$) where the contribution from the radial gradient terms in equation (10) is not negligible. In this case, the angular velocity transition from Ω to Ω_* occurs within δr . The approximate balance between the second term (field generating) and the third (advection) and fourth (dissipation) terms in equation (10) yields a crude estimation for the toroidal field component,

$$B_\phi^+ \approx r (\Omega_* - \Omega) (\delta r) \eta^{-1} B_r^+ \sim r (\Omega_* - \Omega) H \eta^{-1} B_z, \quad (18)$$

provided the width of the boundary layer is assumed to be the electromagnetic screening length for the poloidal magnetic field, i.e. $\delta r \simeq \eta/v_r$ (see GL79). The vertical gradient terms are not taken into account for simplicity in the radial integration of equation (10). The last step in (18) follows from $B_r^+/B_z \sim H/\delta r$ according to equation (14). This analysis indicates that the form of the expression for the azimuthal field component in equation (17) may generally be applicable for the entire disk regardless of the radial extension of the angular velocity transition zone.

In the thin disk limit, the vertically integrated forms of the r and z components of the momentum equation can be written as

$$(\Omega_K^2 - \Omega^2) r H - \frac{B_z B_r^+}{4\pi\rho} \simeq 0, \quad (19)$$

and

$$c_s^2 \simeq \frac{1}{2} \Omega_K^2 H^2 + \frac{(B_\phi^+)^2 + (B_r^+)^2}{8\pi\rho}, \quad (20)$$

where $c_s = (P/\rho)^{1/2}$ is the speed of sound in terms of the mid-plane temperature of the disk, and Ω_K is the Keplerian angular velocity given by

$$\Omega_K(r) = \left(\frac{GM_*}{r^3} \right)^{1/2}, \quad (21)$$

where M_* is the mass of the neutron star. The magnetic tension force in equation (19) is the main agent responsible for the deviation of $\Omega(r)$ from $\Omega_K(r)$ if the accretion disk is thin and the poloidal magnetic field varies on a length scale r . The vertical equilibrium of a magnetically threaded thin disk is given by equation (20), where the gas pressure is balanced by the magnetic pressure of the horizontal field components in addition to the vertical component of gravity. Using equations (19) and (20), it is possible to make an order of magnitude estimate for the sound speed. In the absence of a strong global magnetic field, the rotational profile is nearly Keplerian and $c_s \simeq \Omega_K H$. The rotation of the disk matter at a sub-Keplerian rate can only be realized provided we have

$$\frac{|B_r^+| B}{4\pi\rho} \lesssim \Omega_K^2 H r \quad (22)$$

in equation (19) with $|B_z| \sim B$. If the magnetic diffusivity is turbulent in nature, then the radial component of the magnetic field can be significant, i.e., $|B_r^+| \lesssim B$, and the vertical equilibrium (20) is satisfied by the balance between the gas and magnetic pressures alone,

$$c_s^2 \approx \frac{B^2}{4\pi\rho} \lesssim \Omega_K^2 H r , \quad (23)$$

since the gravity term is relatively small in a thin disk, i.e., $\Omega_K^2 H^2 \ll \Omega_K^2 H r$.

After equation (23), we propose the following prescription for the sound speed:

$$c_s^2 = \xi(r) \Omega_K^2 H r , \quad (24)$$

where $\xi(r) < 1$ is a dimensionless factor of unknown radial dependence. Its explicit form can only be deduced from a detailed analysis of the field configuration and density distribution in the disk.

In this work, we assume that the magnetic diffusivity of the disk is of the same physical origin (i.e., turbulence) as the viscosity, and we adopt the original α formalism (Shakura & Sunyaev 1973, hereafter SS) to write

$$\eta = \alpha_d \frac{c_s^2}{\Omega_K} , \quad (25)$$

where $\alpha_d \lesssim 1$ is a dimensionless numerical factor.

Combining equations (24) and (25), the azimuthal field component at the disk surface (see eq. [17]) is simplified to

$$B_\phi^+ = \gamma_\phi (\Omega_* - \Omega) \Omega_K^{-1} B_z , \quad (26)$$

where $\gamma_\phi \equiv \epsilon/\xi\alpha_d$ will be treated as a constant for simplicity (see, e.g., Livio & Pringle 1992). As we will see in § 3, the vertically integrated dynamical viscosity, $\nu\Sigma$, for a magnetically threaded disk changes with distance. The radial variation of $\nu\Sigma$ can be achieved in general provided both the coefficient of viscosity ν and the surface density Σ are functions of radius. As the viscosity ν and diffusivity η have the same, turbulent nature by assumption, the magnetic Prandtl number, ν/η , should be of order one at different radii of the disk. This also requires that the parameter ξ should have a radial dependence in general for self-consistency. In this case, γ_ϕ would not be approximated as a constant unless the shear reduction factor ϵ changes with distance in more or less the same way as ξ does. Our physical motivation for taking γ_ϕ as a constant is the following. The compressive effect of the magnetic field on the vertical equilibrium of the disk becomes negligible in the weakly magnetized outer disk regions. The gas pressure is mainly balanced by the gravitational force and $c_s \simeq \Omega_K H$

(see eq. [20]). According to equation (24), this is equivalent to choose $\xi(r) \approx H/r$ in the outer disk. The resulting toroidal field is $O(r/H)B_z \gg B_z$ unless $\epsilon(r) \approx H/r$. The shear reduction factor ϵ is therefore expected to decrease from $O(1)$ at small radii to $O(H/r)$ at large radii provided the disk is threaded by the stellar field lines that are closed and stable at least to some extent beyond the corotation radius. As there appears to be a correlation between $\epsilon(r)$ and $\xi(r)$, we approximate their ratio as a constant throughout the entire disk.

In the absence of a complete theory of the disk-star magnetic interaction, we will not attempt to obtain a full disk solution at this stage; we will rather concentrate on the conservation of angular momentum to treat the dynamics of disk accretion under the action of an external magnetic field of stellar origin. Using equation (26), it follows from equation (6) that

$$\frac{d}{dr} \left(2\pi\nu\Sigma r^3 \frac{d\Omega}{dr} + \dot{M} r^2 \Omega \right) = -\gamma_\phi r^2 (\Omega_* - \Omega) \Omega_K^{-1} B_z^2 \quad (27)$$

which can be solved for the rotation profile, $\Omega(r)$, for a given vertically integrated dynamical viscosity, $\nu\Sigma$, if $B_z(r)$ is known.

3. DYNAMICAL VISCOSITY

In the following, we will deal with the angular momentum balance (see § 2) to derive an expression for the vertically integrated dynamical viscosity. Before attempting to solve equation (27), we scale the variable quantities r , $\nu\Sigma$, and Ω by their typical values such that $x \equiv r/r_{\text{in}}$ is a dimensionless coordinate in units of the inner disk radius r_{in} where we assume $\Omega = \Omega_*$, $f(x) \equiv 3\pi\nu\Sigma/\dot{M}$ is a dimensionless function for the dynamical viscosity, and $\omega(x) \equiv \Omega/\Omega_K(r_{\text{in}})$ is a dimensionless angular velocity for the disk plasma. Finally, we use equation (9) for the screened dipole field to rewrite equation (27) in a non-dimensional form:

$$\frac{d}{dx} \left[\frac{2}{3} f(x) x^3 \frac{d\omega}{dx} + x^2 \omega \right] = -\beta (\omega_* - \omega) x^{-5/2}, \quad (28)$$

where $\omega_* \equiv \Omega_*/\Omega_K(r_{\text{in}}) = (r_{\text{co}}/r_{\text{in}})^{-3/2}$ with the corotation radius $r_{\text{co}} = (GM_*/\Omega_*^2)^{1/3}$ and $\beta \equiv \gamma_\phi s_{\text{eff}}^2 (r_A/r_{\text{in}})^{7/2}$ with the Alfvén radius given by

$$\begin{aligned} r_A &= \dot{M}^{-2/7} \mu_*^{4/7} (GM_*)^{-1/7} \\ &\simeq 3.4 \times 10^8 \text{ cm } \dot{M}_{17}^{-2/7} \mu_{*30}^{4/7} \left(\frac{M_*}{1.4 M_\odot} \right)^{-1/7}. \end{aligned} \quad (29)$$

Here, \dot{M}_{17} is the mass accretion rate expressed in units of 10^{17} g s^{-1} and μ_{*30} is the magnetic dipole moment in units of 10^{30} G cm^3 . If the neutron star magnetic field is sufficiently weak

for a given mass accretion rate, e.g., $B_* \lesssim 10^7$ G in equation (29), then we have $r_A < R_*$ and the disk may extend down to the surface of the central object (i.e., $r_{\text{in}} = R_*$). For such weakly magnetized systems also known as the standard α -disks (SS), we get $\beta \simeq 0$. The same is true also if the disk plasma is perfectly diamagnetic. In the conventional picture of α -disks, the rotation curve is Keplerian throughout the accretion flow except in a narrow boundary layer situated at the inner edge of the disk where the angular velocity of the plasma changes from $\Omega_K(R_*)$ to Ω_* . In a standard thin disk around a non-magnetic star, we can integrate equation (28) with $\beta = 0$ to find $f(x) = 1 - \zeta x^{-1/2}$ using the Keplerian profile, $\omega(x) = x^{-3/2}$. The integration constant ζ , here, denotes the inflow rate of angular momentum \dot{J} , across a cylindrical boundary at radius r , in terms of the angular momentum flux carried by matter onto the neutron star through the inner edge of the disk, i.e., $\dot{J} = \zeta \dot{M} R_*^2 \Omega_K(R_*)$. According to the standard approach (Lynden-Bell & Pringle 1974), there is no viscous torque acting on the inner disk. This corresponds to $\zeta \simeq 1$ and the boundary layer is extremely thin in extension. However, the angular velocity transition region is not necessarily narrow as Glatzel showed (Glatzel 1992, hereafter G92) if ζ is treated as a free parameter in $f(x)$, which in turn can be used to solve for the structure of the accretion flow (Fujimoto 1995). In the present investigation, we will derive a form of vertically integrated dynamical viscosity in a way similar to the work of G92 but generalized to treat the disk interacting with a magnetic star. In our case, $\beta \neq 0$ and the angular momentum exchange between the magnetosphere and the disk is not negligible except for sufficiently large distances from the magnetically braked inner disk regions. The Keplerian rotation can only be regarded as a particular solution that can be employed to obtain a prescription for the dynamical viscosity, which may hold throughout the accretion flow provided the angular motion of the inner disk plasma can be matched to the rotation rate of the stellar magnetosphere. The radial integration of equation (28) for a Keplerian angular velocity profile yields

$$f(x; \beta, j, \omega_*) = 1 - \frac{2}{3}\beta\omega_*x^{-2} + \frac{1}{3}\beta x^{-7/2} - jx^{-1/2}, \quad (30)$$

where $j \equiv \dot{J}/\dot{M}r_{\text{in}}^2\Omega_K(r_{\text{in}})$ is the net angular momentum flux into the neutron star unless there are some other efficient mechanisms of angular momentum loss for the disk material such as winds associated with the opening of field lines. Although j , here, appears to be an arbitrary integration constant, it is the dimensionless torque applied by the disk on the star, i.e., the star spins up (or spins down) for $j > 0$ (or $j < 0$).

A vertically integrated dynamical viscosity form similar to the one we consider in equation (30) was derived and used previously by Brandenburg & Campbell (1998, hereafter BC98) to solve for the disk structure around strongly magnetic accretors. These authors, however, assumed $j = 0$ to ensure that the disk structure matches that of weakly magnetized accretion at a sufficiently large radius r_{out} . Adopting $\nu\Sigma = \dot{M}/3\pi$, that is,

$f(x = r_{\text{out}}/r_{\text{in}}) = 1$ as an arbitrary outer boundary condition, they integrated the relevant MHD equations in the radial direction from the outer disk regions inwards. Note that $f = 1$ at large distances whether $j = 0$ or not. However, the structure at finite x depends on the relative importance of the terms, and the value of j will be an important parameter in determining the structure. BC98 did not attempt to fit their solution to a magnetically braked inner accretion flow; they assumed that the Keplerian rotation holds throughout the disk. Their model implies that the torque on the star is always zero, i.e., $j = 0$, and the angular velocity of the plasma still remains Keplerian in the inner parts of the disk even though the viscous dissipation there due to magnetically enhanced viscous stress (see the third term on the r.h.s. of eq. [30]) leads to the divergence of the disk height as a result of elevated temperature. Both assumptions are very restrictive and non-physical in the sense that the choice of j becomes quite significant at small radii although it seems to have no effect on the disk structure at large radii (see § 4) and the huge viscous dissipation estimated for the inner disk regions results from using overestimated angular frequencies (e.g., Keplerian frequencies) together with a magnetically enhanced dynamical viscosity. The last argument can be made clear if we consider the conservation of energy for a radiatively efficient disk,

$$2\sigma T_s^4 \approx \int_{-H}^H Q_v dz = \frac{GM_*\dot{M}}{3\pi r_{\text{in}}^3} \left(x \frac{d\omega}{dx}\right)^2 f(x; \beta, j, \omega_*) , \quad (31)$$

where T_s is the effective surface temperature of the disk and $Q_v = \nu\rho(r\partial_r\Omega)^2$ is the viscous dissipation rate per unit volume. The approximation sign in equation (31) indicates that there may exist additional sources of heat (e.g., Ohmic dissipation) other than viscosity in the disk. If the Keplerian assumption, i.e., $\omega(x) = x^{-3/2}$, were valid throughout the entire disk as in the work of BC98, then we would certainly find huge temperatures as $x \rightarrow 1$ for sufficiently high β and low ω_* values (see, e.g., CH98 for the corresponding values) in the case of $j = 0$ (see also, eq. [30]).

What we expect to find in steady accretion is that the inner boundary condition, that is, the fastness of the stellar magnetosphere ω_* , adjusts the rotational disk dynamics for a given torque j . The quantity β in equation (30), which reflects the magnetic configuration in the inner disk, is not an independent parameter. Rather, it is linked intimately to j and its value can be calculated (see § 4) when the angular velocity profile is determined from equation (28).

The definition of β with $r_{\text{in}} = \omega_*^{2/3} r_{\text{co}}$, yields for a typical X-ray binary pulsar:

$$\beta \simeq 12 \gamma_\phi s_{\text{eff}}^2 \omega_*^{-7/3} \dot{M}_{17}^{-1} P_*^{-7/3} \mu_{*30}^2 \left(\frac{M_*}{1.4 M_\odot}\right)^{-5/3} , \quad (32)$$

where P_* is the spin period of the neutron star. Using the torque expression, $N_* = I_*\dot{\Omega}_* =$

$j\dot{M}(GM_*r_{\text{in}})^{1/2}$ with a moment of inertia $I_* = (2/5) M_* R_*^2$, we find

$$j \simeq -0.4 \omega_*^{-1/3} \dot{M}_{17}^{-1} P_*^{-7/3} R_{*6}^2 \left(\frac{\dot{P}_*}{10^{-12} \text{ s s}^{-1}} \right) \times \left(\frac{M_*}{1.4 M_\odot} \right)^{1/3}, \quad (33)$$

where R_{*6} is the neutron star radius expressed in units of 10^6 cm and \dot{P}_* is the time rate of change of the spin period.

We now examine some of the basic features of the dimensionless function we introduced for the dynamical viscosity (see eq. [30]) before we present various types of rotation profiles in the next section, for the behavior of $\omega(x)$ strongly depends on $f(x)$ and its first derivative $f'(x)$ (see eq. [28]). As an illustrative example of how the dimensionless viscosity is affected by the last term in equation (30), we display in Figure 1 plots of $f(x)$ for two different values of j . The dynamical viscosity function shown by the solid curve in Figure 1 corresponds to $\beta = 16$, $\omega_* = 0.6$, and $j = -0.8$. According to equations (32) and (33), this can be realized for a typical X-ray binary pulsar of spin period 1 s if $\gamma_\phi \simeq 0.4$ with $s_{\text{eff}} \simeq 1$ and $\dot{P}_* \simeq 1.7 \times 10^{-12} \text{ s s}^{-1}$. The dashed curve (see Fig. 1) with $\beta = 13$, $\omega_* = 0.3$, and $j = 0.9$, represents another physically plausible dynamical viscosity for the same pulsar provided $\gamma_\phi \simeq 0.1$ for $s_{\text{eff}} \simeq 0.8$ and $\dot{P}_* \simeq -1.5 \times 10^{-12} \text{ s s}^{-1}$. Note that the curve associated with a negative value of j (spin-down) is characterized by two local extrema, corresponding to a maximum and a minimum, located respectively at x_2 and x_1 , with $x_1 < x_2$. Also, note that there is no local maximum for $j > 0$. The curves in Figure 1 are plotted for illustrative values of β and ω_* . The conclusions drawn from Figure 1 however can be generalized also for other values of β and ω_* , if we consider the sign of the second derivative of $f(x)$ at local extrema. The real extremum points, $x_{\text{ext}} = x_{1,2}$, can be found from $f'(x_{\text{ext}}) = 0$ as

$$x_{1,2} = \frac{1}{9j^2} \left[\left(-36\beta\omega_* \pm 9\sqrt{16\beta^2\omega_*^2 + 21\beta j} \right) j^2 \right]^{2/3}, \quad (34)$$

provided we have $16\beta\omega_*^2 + 21j \geq 0$. The first root, x_1 , specified by the plus sign within the parenthesis in equation (34) can be identified to be the local minimum, whereas the second root, x_2 , with minus sign represents the local maximum. Equation (34) then, implies that $x_1 < x_2$. The local minima of both curves in Figure 1 are inside the corotation radii, i.e., $x_1 \simeq 1.3 < x_{\text{co}} \simeq 1.4 < x_2 \simeq 9.8$ for $\omega_* = 0.6$ and $x_1 \simeq 1.8 < x_{\text{co}} \simeq 2.2$ for $\omega_* = 0.3$, where $x_{\text{co}} \equiv r_{\text{co}}/r_{\text{in}}$. As we will see in § 4, $x_1 < r_{\text{co}}/r_{\text{in}}$ is always satisfied if the rotation of the disk matter is nearly Keplerian for $r \geq r_{\text{co}}$. The plasma is progressively brought into corotation with the neutron star in an inner transition zone of radial extension δr_{in} . The angular velocity of the inner disk matter starts deviating from its Keplerian value at $r \lesssim x_1 r_{\text{in}}$, for

the magnetic stress dominates over the shear stress when the dynamical viscosity becomes sufficiently small, that is, when $f(x_1) \ll 1$. The width of the inner transition zone can be then estimated as $\delta \lesssim x_1 - 1$.

4. APPLICATION TO OBSERVED BINARY X-RAY PULSARS

We solved the second order differential equation (28) for $\omega(x)$, substituting equation (30) for the dynamical viscosity. As we do not know a priori where the true inner disk radius is located, we tried different values of ω_* for a given torque j . As an initial guess for each set of (ω_*, j) , we calculated β such that $f(x_1) = 0$. We observed that the necessary boundary conditions, i.e., $\omega(x = 1) = \omega_*$ and $\omega(x > x_{\text{co}}) \simeq x^{-3/2}$, are satisfied to the desired accuracy in our numerical iteration only for certain values of β for which the dynamical viscosity nearly vanishes at $x = x_1$. Our results for a rotator in spin equilibrium, i.e., $j = 0$, are shown in Figures 2a and 2b. As in Figure 1, the corresponding dynamical viscosities (dashed curves) and the angular velocity profiles (solid curves) are plotted as functions of $x = r/r_{\text{in}}$. The dotted curves represent Keplerian rotation. Note that the angular velocity is braked by the magnetic stress only inside x_{co} , and the rotation of the disk plasma is almost Keplerian outside x_{co} . We calculate the net torque applied by the disk on the star using a closed surface through the corotation radius. The surface encloses the central object and excludes part of the disk for $x \geq x_{\text{co}}$. This choice avoids the uncertainties involved in making torque calculations in the inner disk where $\Omega \neq \Omega_{\text{K}}$. We write the torque as

$$N_* = N_{\text{co}}^{\text{mat}} + N_{\text{co}}^{\text{vis}} + N_{\text{mag}} , \quad (35)$$

where the angular momentum flux carried by the material stress through a cylindrical surface area $4\pi r_{\text{co}} H(r_{\text{co}})$ is

$$N_{\text{co}}^{\text{mat}} = \dot{M} r_{\text{co}}^2 \Omega_{\text{K}}(r_{\text{co}}) . \quad (36)$$

The contribution of the viscous stress to the flux of angular momentum through the same surface is given by

$$\begin{aligned} N_{\text{co}}^{\text{vis}} &= \frac{\dot{M}}{3\pi} f(x_{\text{co}}) r_{\text{co}}^2 \left(\frac{d\Omega_{\text{K}}}{dr} \right)_{r_{\text{co}}} (2\pi r_{\text{co}}) \\ &= -f(x_{\text{co}}) \dot{M} r_{\text{co}}^2 \Omega_{\text{K}}(r_{\text{co}}) . \end{aligned} \quad (37)$$

The magnetic coupling outside the corotation radius yields a net spindown torque,

$$N_{\text{mag}} = - \int_{r_{\text{co}}}^{\infty} r^2 B_z B_{\phi}^+ dr = -\frac{1}{3} \beta x_{\text{co}}^{-7/2} \dot{M} r_{\text{co}}^2 \Omega_{\text{K}}(r_{\text{co}}) \quad (38)$$

which, together with equations (36) and (37), gives $N_* = j\dot{M}(GM_*r_{\text{in}})^{1/2}$ according to equation (30). This justifies our interpretation of j as the dimensionless torque acting on the neutron star in units of the angular momentum flux carried by matter through the inner edge of the disk. Also, note from Figures 2a and 2b that x_1 decreases (i.e., $x_1 \rightarrow 1$) while ω_* increases as expected. There is, however, an upper limit for ω_* if the star is in rotational equilibrium since

$$\lim_{j \rightarrow 0} x_1(\beta, j, \omega_*) = \left(\frac{7}{8\omega_{*,c}} \right)^{2/3} \geq 1, \quad (39)$$

independent of β , following from equation (34). Thus, for accreting systems in rotational equilibrium, $j = 0$, the critical fastness parameter $\omega_{*,c}$ for the transition from spin-down to spin-up depends on the angular velocity profile (width of the transition zone) in equilibrium. Equation (39) implies that the maximum possible critical fastness parameter is $(\omega_{*,c})_{\text{max}} = 0.875$, a value quoted previously by Wang (1995, hereafter W95) as the critical fastness parameter for a star accreting from a turbulent disk. According to the accretion torque model of W95, the Keplerian rotation holds throughout the whole disk. Equivalently, in our model, this maximum critical fastness parameter obtains if the angular velocity transition region is extremely narrow or there is no transition region at all. This corresponds to the $x_1 = 1$ limit among systems in spin equilibrium as seen from the comparison of Figures 2a and 2b. The usual fastness parameter, ω_s , can be expressed in terms of ω_* as

$$\omega_s \equiv \frac{\Omega_*}{\Omega_K(r_0)} = \left(\frac{r_0}{r_{\text{co}}} \right)^{3/2} = x_0^{3/2} \omega_*. \quad (40)$$

Here, r_0 is the radius where Ω reaches its maximum and $x_0 \equiv r_0/r_{\text{in}}$. Using equation (40), we obtain $\omega_{s,c} \cong 0.75$ for $\omega_{*,c} = 0.5$ from Figure 2a and $\omega_{s,c} \cong 0.83$ for $\omega_{*,c} = 0.8$ from Figure 2b. Our analysis indicates broad transition zones for $j = 0$ rather than narrow ones if $\omega_{s,c} < 0.8$. The disk is Keplerian at all radii only for $\omega_{*,c} = \omega_{s,c} = 0.875$ and $x_0 = x_1 = 1$.

We have extended our calculations to several binary X-ray pulsars observed as QPO sources. One of the simplest and most frequently used models for QPOs from X-ray pulsars is the beat frequency model (Alpar & Shaham 1985). According to the beat frequency model (BFM), the inhomogeneities at the inner edge of the Keplerian disk modulate the X-ray intensity and the QPO is observed as the beat frequency between the local Keplerian frequency and the neutron star spin frequency,

$$\nu_{\text{QPO}} = \nu_K(r_0) - \nu_*. \quad (41)$$

The corresponding fastness parameter can be written as

$$\omega_s^{\text{BFM}} = \frac{1}{1 + P_* \nu_{\text{QPO}}}, \quad (42)$$

where P_* is the spin period of the observed X-ray pulsar. The QPOs detected from X-ray pulsars can be used, within the beat frequency model, to obtain constraints on the fastness parameter. For each source, we assumed $M_* = 1.4 M_\odot$ and $R_{*6} = 1$. We calculated j as a function of ω_* from equation (33) and ω_s^{BFM} from equation (42) using the observed periods P_* , period derivatives \dot{P}_* , X-ray luminosities L_X , and QPO frequencies ν_{QPO} of these X-ray pulsars (Takeshima et al. 1994; Wang 1996, and references therein). We determined the mass accretion rates through $\dot{M} = L_X R_*/GM_*$. The magnetic dipole moments μ_{*30} have been recently deduced from the cyclotron features (Coburn et al. 2002). Sources like 4U 1626 – 67, which are known to be close to their spin equilibrium, indicate lower values for the critical fastness parameter. The reason for this could be the deviation of angular velocity from the Keplerian profile near the inner disk regions (Li & Wang 1996). Figure 3a shows the predicted rotation curve of 4U 1626 – 67 when the pulsar was spinning up just before the torque reversal in 1990. After the torque reversal, we expect the angular motion of the disk matter around the same pulsar as in Figure 3b. The estimated angular velocity profiles of 4U 0115 + 63 and Cen X-3 are plotted in Figures 4 and 5, respectively. We could obtain the relevant rotation profiles shown in Figures 3, 4, and 5 only for specific values of ω_* provided we have $\omega_s = \omega_s^{\text{BFM}}$ (see eq. [40]). With these constraints, the disk model depends on three parameters, r_{in} , β and j , and there is a unique solution, such that if one of these three parameters is known, the other two can be obtained as the parameters that yield the unique solution for $\Omega(r)$. For example, if the value of r_{in} is assumed, e.g., $r_{\text{in}} = r_A$, then β and j , therefore the torque on the star can be obtained; numerically by scanning the β, j parameter space until the unique solution is found. In the applications, we used observed values of $\dot{\Omega}$ to determine j and scanned in β only, to use a shortcut to the model solution. We now summarize our results for each of these individual sources.

4U 1626 – 67 is a low-mass X-ray binary pulsar with a 7.66 s spin period. The pulsar was in a steady spin-up state with $\dot{P}_* \cong -4.86 \times 10^{-11} \text{ s s}^{-1}$ during 1977 – 1990. After the 1990 torque reversal, the source underwent steady spin-down with $\dot{P}_* \cong 4.32 \times 10^{-11} \text{ s s}^{-1}$. Although there is no indication for an abrupt change in the X-ray luminosity at the torque reversal, a gradual decrease over a decade in the mass accretion rate can be seen from the archival flux history (Chakrabarty et al. 1997). The QPO frequency is $\sim 0.04 \text{ Hz}$ during both the spin-up and spin-down episodes. The estimated mass accretion rates are $\dot{M}_{17} \approx 1$ for spin-up and $\dot{M}_{17} \approx 0.5$ for spin-down. The beat frequency model gives $\omega_s^{\text{BFM}} = 0.76$. Figure 3a shows the predicted rotation curve, when the pulsar spins up, for $\omega_s \cong 0.76$ with $\omega_* = 0.65$ and $\beta = 6.48$. The angular velocity profile during the spin-down episode was estimated for the same fastness parameter as in Figure 3b with $\omega_* = 0.2$ and $\beta = 163$. We find $r_{\text{in}}/r_{\text{co}} \cong 0.75$ and $r_{\text{in}}/r_0 \cong 0.91$ for spin-up, and $r_{\text{in}}/r_{\text{co}} \cong 0.34$ and $r_{\text{in}}/r_0 \cong 0.41$ for spin-down with $r_{\text{co}} \cong 6.5 \times 10^8 \text{ cm}$. At the torque reversal, we expect that $\gamma_\phi s_{\text{eff}}^2$ changes

from 4.7 to 3.8 according to our values of β and ω_* for $\mu_{*30} = 2.2$. Note that the angular velocity transition zone is quite broad for the spin-down state, i.e., $\delta r/r_0 = 1 - r_{\text{in}}/r_0 \cong 0.59$ in comparison with $\delta r/r_0 \cong 0.09$ during the spin-up episode.

4U 0115 + 63 is a 3.61 s pulsar. It has $\dot{P}_* \cong -3.66 \times 10^{-12} \text{ s s}^{-1}$ and $\dot{M}_{17} \approx 0.43$. The observed QPO frequency is 0.062 Hz. We inferred a fastness parameter of 0.817 from the beat frequency model. We find $r_0 \cong 3.4 \times 10^8 \text{ cm}$ and $r_{\text{co}} \cong 3.9 \times 10^8 \text{ cm}$. The same value for ω_s can be determined from the angular velocity profile if $\omega_* = 0.78$ (see Fig. 4). We get $r_{\text{in}}/r_0 \cong 0.97$. The width of the transition zone can be estimated as $\delta r/r_0 \cong 0.03$. An Alfvén radius of $4.3 \times 10^8 \text{ cm}$ for $\mu_{*30} \cong 1$ gives $r_{\text{in}}/r_A \cong 0.77$. The solution in Figure 4 was obtained for $\beta = 4.25$. This further implies that $\gamma_\phi s_{\text{eff}}^2 \cong 1.7$.

Cen X-3 is a 4.83 s pulsar. It has $\dot{P}_* \cong -4.29 \times 10^{-11} \text{ s s}^{-1}$ and $\dot{M}_{17} \approx 4.3$. The observed QPO frequency is 0.035 Hz. The fastness parameter inferred from equation (42) is 0.855. We estimate $r_0/r_{\text{co}} \cong 0.9$. A boundary layer width of $\delta r/r_0 \cong 0.01$ can be deduced from $r_{\text{in}}/r_0 \cong 0.99$. Our computation gives $\omega_s = 0.855$ only for $\omega_* = 0.84$ and $\beta = 3.92$ (see Fig. 5). This yields $r_{\text{in}} \cong 4.27 \times 10^8 \text{ cm}$ and $\gamma_\phi s_{\text{eff}}^2 \cong 14$ for $\mu_{*30} \cong 2$ and $r_{\text{co}} \cong 4.8 \times 10^8 \text{ cm}$. Our model predicts $r_{\text{in}}/r_A \cong 1.28$ for this source.

5. MODEL APPLICATIONS IN COMPARISON WITH RESULTS OF NUMERICAL SIMULATIONS

The recent numerical study made by RUKL02 is the only work where the slow viscous accretion and the disk-magnetized star interaction were investigated in full two-dimensional time-dependent simulations with quasi-stationary conditions. The results of RUKL02 are relevant to all stationary models that describe the magnetic interaction of an accreting star with its surrounding disk. As the simulations by RUKL02 are two-dimensional whereas our work is limited to one-dimension, we expect significant differences between some of our results and their predictions. The inner boundary chosen by RUKL02 to investigate the dynamics of disk accretion is the rotating star on which free boundary conditions are applied to several hydrodynamic variables. In our work, the computational region is limited by the inner radius of the disk where the disk plasma corotates with the stellar magnetosphere. We keep the Keplerian law fixed as the asymptotic outer boundary condition on the rotation rate of the disk matter. The outer boundary conditions taken by RUKL02 on all hydrodynamic variables are fixed for the maximum computational region and free for a smaller simulation region (inner disk).

Although our boundary conditions differ significantly from the ones used by RUKL02,

it is possible to make appropriate conversions between our reference values and those of RUKL02 for the inner disk radius and the physical quantities such as the stellar rotation rate and the angular momentum flux. Our reference value for the distance is always the true inner radius of the disk, r_{in} , which is equivalent to one in dimensionless units. The innermost disk radius within which all the disk matter goes up into the funnel flow changes in time relative to the reference value for the distance, R_0 , in numerical simulations of RUKL02. This innermost radius corresponds to r_{in} in our model since the matter nearly corotates with the star inside $r_{\text{in}} < R_0$.

The dimensionless stellar rotation rate, that is the fastness parameter in our units is given by

$$\omega_* \equiv \omega_{*0} \left[\frac{\Omega_{\text{K}}(R_0)}{\Omega_{\text{K}}(r_{\text{in}})} \right] = \omega_{*0} \left(\frac{r_{\text{in}}}{R_0} \right)^{3/2}, \quad (43)$$

where ω_{*0} is the fastness parameter in units of RUKL02.

The dimensionless total angular momentum flux to the star in our units can be written as

$$j \equiv \frac{\dot{J}}{\dot{M} r_{\text{in}}^2 \Omega_{\text{K}}(r_{\text{in}})} = \varphi \left(\frac{\dot{M}_0}{\dot{M}} \right) \left(\frac{R_0}{r_{\text{in}}} \right)^{1/2}, \quad (44)$$

where $\dot{J} = \varphi \dot{M}_0 R_0^2 \Omega_{\text{K}}(R_0)$ is the total angular momentum flux to the star and \dot{M}_0 is the reference mass accretion rate in units of RUKL02.

In the following, we will estimate the approximate location of the braking radius r_{br} , using our model parameters β , j , and ω_* . The braking radius was first defined by RUKL02 as the radius inside which the disk is significantly disturbed by the stellar field. In almost all simulations by RUKL02 (especially the relevant ones with ‘‘Type I’’ initial conditions), the density in the disk drops sharply at $r \lesssim r_{\text{br}}$ and the matter is magnetically braked for $r_{\text{in}} < r \lesssim r_{\text{br}}$. The density in the disk rises again near the innermost radius. The radial variation of density at each time step of these numerical simulations is qualitatively reminiscent of the behavior of our dynamical viscosity, $f(x) = 3\pi\nu\Sigma/\dot{M}$ (see Fig. 1). To make a quantitative comparison of our model predictions with the results of RUKL02, we use the numerical data of simulations for accretion to a slowly rotating star with $\omega_{*0} = 0.19$. We select the numerical values given by RUKL02 for the mass accretion rate \dot{M}/\dot{M}_0 , the angular momentum flux φ , and the inner disk radius r_{in}/R_0 at times $t = 30P_0$ and $t = 40P_0$, where P_0 is the rotational period at R_0 . Using equations (43) and (44), we calculate our model parameters ω_* and j . Equations (30) and (34) can be employed together with the condition $f(x_1) \ll 1$ (see §§ 3 and 4) to solve for β . Once all model parameters are determined, the braking radius $r_{\text{br}} \approx (r_{\text{in}}/R_0)x_1$ where the density becomes minimum can be readily found from equation (34). Our numerical calculations yield $r_{\text{br}} \approx 2.61$ at $t = 30P_0$ and $r_{\text{br}} \approx 2.65$

at $t = 40P_0$. These estimates are in agreement with the results of RUKL02.

6. DISCUSSION

We investigated the rotational dynamics of an accretion disk threaded by the dipolar magnetic field of a neutron star with constant screening factor. Within model assumptions, we found that a range of narrow or wide angular velocity transition zones with non-Keplerian rotation are consistent with observations. Our approach is analogous to the work of Glatzel (1992) for the non-magnetic case. We derived a vertically integrated dynamical viscosity form for a magnetically threaded disk from the conservation of mass and angular momentum using the Keplerian rotation as a particular solution for the angular motion of the disk plasma. Assuming that the whole disk can be treated by the same dynamical viscosity, we were able to obtain rotation curves without the restricting assumption of a thin boundary layer. We also used a more realistic, spatially varying azimuthal pitch, B_ϕ^+/B_z , throughout the angular velocity transition zone instead of keeping it constant as in the model of Ghosh & Lamb. The effect of the magnetically enhanced viscous stress is included in our calculations. The rotation of the disk matter is almost Keplerian outside the corotation radius. The deviation from the Keplerian law is noticeable where the effective viscous stress is negligible as compared with the magnetic stress. This can be realized at a specific disk radius, $r_1 = x_1 r_{\text{in}}$, where the vertically integrated dynamical viscosity function, f , goes through a local minimum and actually nearly vanishes. The angular velocity at r_1 is still nearly Keplerian. We find that the angular motion of the inner disk plasma from r_1 to r_{in} is controlled by both the viscous and magnetic stresses. The true inner disk radius, r_{in} , is therefore determined in our model by the close balance between the magnetic stress and the viscous and material stresses. The width of the transition zone, $\delta \lesssim x_1 - 1$, depends basically on the model parameters β , j , and ω_* (see §§ 3 and 4). The physical meaning of this is that for different values of \dot{M} , Ω_* and for given μ_* , the torque on the star from a disk threaded by a screened dipole field can be achieved with the adjustment of the $\Omega(r)$ profile through a transition zone. The rotation is nearly Keplerian throughout the whole disk and the angular velocity transition region is narrow in the case of dynamical viscosity decreasing towards the innermost edge of the disk for the current values of β , j , and ω_* . The boundary layer approximation of GL79 remains valid only for $f(x \simeq 1) \approx 0$ (see Fig. 5). In this sense, the viscously unstable inner disk solutions of BC98 and CH98 could be an artefact of taking a fully Keplerian disk. In general the inner disk is not Keplerian; the angular momentum transfer with a dynamical viscosity increasing at small radii cannot satisfy the boundary condition imposed by the rotating magnetosphere if the inner disk is assumed to be Keplerian (see Fig. 3b).

Using observed parameters of several sources in equilibrium, spin-up or spin-down states, we found that the non-Keplerian transition region for a Keplerian flow to match to the rotation rate of the stellar magnetosphere can be broad or narrow depending on source state. The beat frequency interpretation of QPOs provides a constraint on the fastness parameter for a given source, and thus on the model parameters (β, j, ω_*) that determine the appropriate rotation curve and the width of the transition zone. Among the examples we considered, the transition zones are narrowest, $\delta r/r_0 \sim 0.01 - 0.1$ for sources in spin-up (4U 1626 – 67, 4U 0115 + 63, Cen X-3); while $\delta r/r_0 \sim 0.02 - 0.24$ for sources in rotational equilibrium; and broadest, $\delta r/r_0 \sim 0.6$ for 4U 1626 – 67, when the source is in spin-down state. QPOs from disk-fed torque reversing X-ray binary pulsars may elucidate the function of non-Keplerian accretion flows and/or the width of the transition zones in the spin behavior of these sources.

Results of the numerical simulations by RUKL02 were compared to our model. These two-dimensional simulations describe an analogous situation where the disk is threaded by the magnetic field of the star; both viscosity and diffusivity are of the same order of magnitude; and the disk matter slowly accretes across the field lines. Although the direct comparison of the angular velocity distributions is not possible because of different conditions assumed at the boundaries of computational domains; there are remarkable similarities between our model predictions and the results of RUKL02 (see § 5).

We thank the anonymous referee for constructive comments and suggestions, K. Y. Ekşi, F. K. Lamb, and H. Spruit for useful discussions, and E. N. Ercan for her support and encouragement. This work was supported by Boğaziçi University Research Foundation under code 01B303D for M. H. E., by the Sabancı University Astrophysics and Space Forum, by the High Energy Astrophysics Working Group of TÜBİTAK (The Scientific and Technical Research Council of Turkey) and by the Turkish Academy of Sciences for M. A. A.

REFERENCES

- Alpar, M. A., & Shaham, J. 1985, *Nature*, 316, 239
- Aly, J. J. 1980, *A&A*, 86, 192
- Aly, J. J., & Kuijpers, J. 1990, *A&A*, 227, 473
- Basri, G., & Bertout, C. 1989, *ApJ*, 341, 340
- Brandenburg, A., & Campbell, C. G. 1998, *MNRAS*, 298, 223

- Campbell, C. G. 1992, *Geophys. Astrophys. Fluid Dyn.*, 63, 179
- Campbell, C. G., & Heptinstall, P. M. 1998, *MNRAS*, 299, 31
- Chakrabarty, D., Bildsten, L., Grunsfeld, J. M., Koh, D. T., Prince, T. A., Vaughan, B. A., Finger, M. H., Scott, D. M., & Wilson, R. B. 1997, *ApJ*, 474, 414
- Coburn, W., Heindl, W. A., Rothschild, R. E., Gruber, D. E., Kreykenbohm, I., Wilms, J., Kretschmar, P., & Staubert, R. 2002, *ApJ*, 580, 394
- Fujimoto, M. Y. 1995, *ApJ*, 450, 262
- Ghosh, P., & Lamb, F. K. 1978, *ApJ*, 223, L83
- Ghosh, P., & Lamb, F. K. 1979, *ApJ*, 232, 259
- Glatzel, W. 1992, *MNRAS*, 257, 572
- Goodson, A. P., Böhm, K. H., & Winglee, R. 1999, *ApJ*, 524, 142
- Goodson, A. P., Winglee, R., & Böhm, K. H. 1997, *ApJ*, 489, 199
- Hayashi, M. R., Shibata, K., & Matsumoto, R. 1996, *ApJ*, 468, L37
- Ichimaru, S. 1978, *ApJ*, 224, 198
- Joss, P. C., & Rappaport, S. A. 1984, *ARA&A*, 22, 537
- Li, X. -D., & Wang, Z. -R. 1996, *A&A*, 307, L5
- Livio, M., & Pringle, J. E. 1992, *MNRAS*, 259, 23P
- Lovelace, R. V. E., Romanova, M. M., & Bisnovatyi-Kogan, G. S. 1995, *MNRAS*, 275, 244
- Lovelace, R. V. E., Romanova, M. M., & Newman, W. I. 1994, *ApJ*, 437, 136
- Lynden-Bell, D., & Boily, C. 1994, *MNRAS*, 267, 146
- Lynden-Bell, D., & Pringle, J. E. 1974, *MNRAS*, 168, 603
- Miller, K. A., & Stone, J. M. 1997, *ApJ*, 489, 890
- Romanova, M. M., Ustyugova, G. V., Koldoba, A. V., Chechetkin, V. M., & Lovelace, R. V. E. 1998, *ApJ*, 500, 703

- Romanova, M. M., Ustyugova, G. V., Koldoba, A. V., & Lovelace, R. V. E. 2002, *ApJ*, 578, 420
- Scharlemann, E. T. 1978, *ApJ*, 219, 617
- Shakura, N. I., & Sunyaev, R. A. 1973, *A&A*, 24, 337
- Takehima, T., Dotani, T., Mitsuda, K., & Nagase, F. 1994, *ApJ*, 436, 871
- Wang, Y. -M. 1987, *A&A*, 183, 257
- Wang, Y. -M. 1995, *ApJ*, 449, L153
- Wang, Y. -M. 1996, *ApJ*, 465, L111
- Warner, B. 1995, *Cataclysmic Variable Stars* (Cambridge: Cambridge Univ. Press)

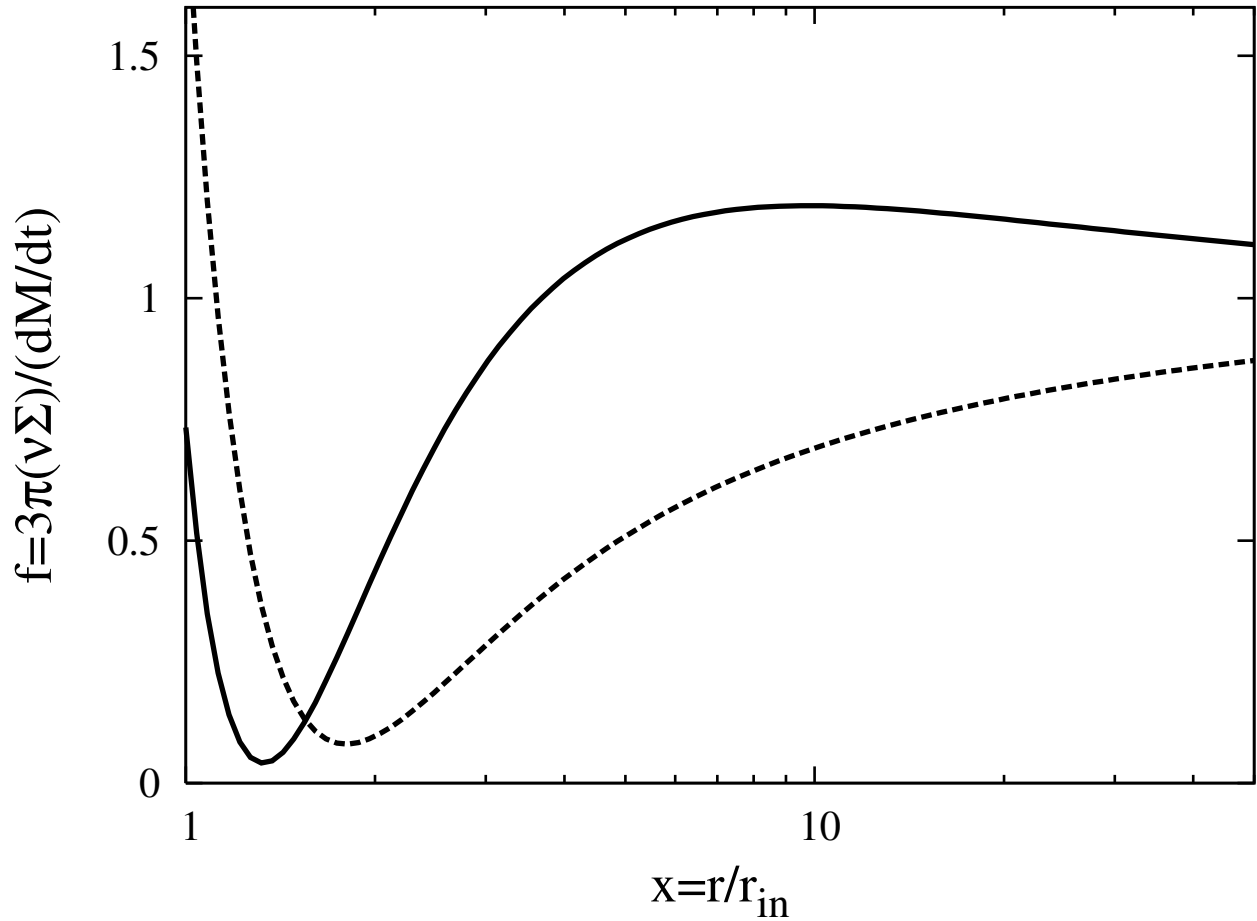


Fig. 1.— Radial variation of normalized vertically integrated dynamical viscosity $f(x) = 3\pi\nu\Sigma/\dot{M}$ from the outer disk regions $x = 50$ to the innermost radius $x = 1$, where $x \equiv r/r_{\text{in}}$, for different values of parameters (β, j, ω_*) . The *solid curve* corresponds to $f(x)$ with $\beta = 16$, $\omega_* = 0.6$, and $j = -0.8$ and the *dashed curve* to $f(x)$ with $\beta = 13$, $\omega_* = 0.3$, and $j = 0.9$.

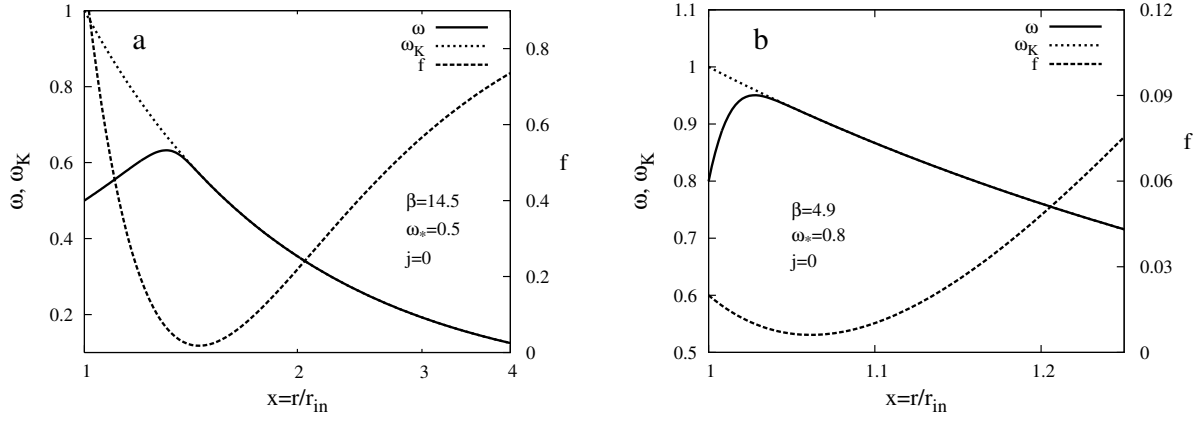


Fig. 2.— Radial variation of angular velocity $\omega(x) \equiv \Omega/\Omega_K(r_{\text{in}})$ and the corresponding normalized vertically integrated dynamical viscosity $f(x) = 3\pi\nu\Sigma/\dot{M}$ for a disk around a magnetized star in spin equilibrium. The rotation rate profiles $\omega(x)$ shown by *solid curves* in panels (a) and (b) obtain for $\beta = 14.5$, $\omega_* = 0.5$, $j = 0$ and $\beta = 4.9$, $\omega_* = 0.8$, $j = 0$, respectively. In each panel the *dashed curve* corresponds to $f(x)$ and the *dotted curve* to the Keplerian profile $\omega_K(x) = x^{-3/2}$, where $x \equiv r/r_{\text{in}}$.

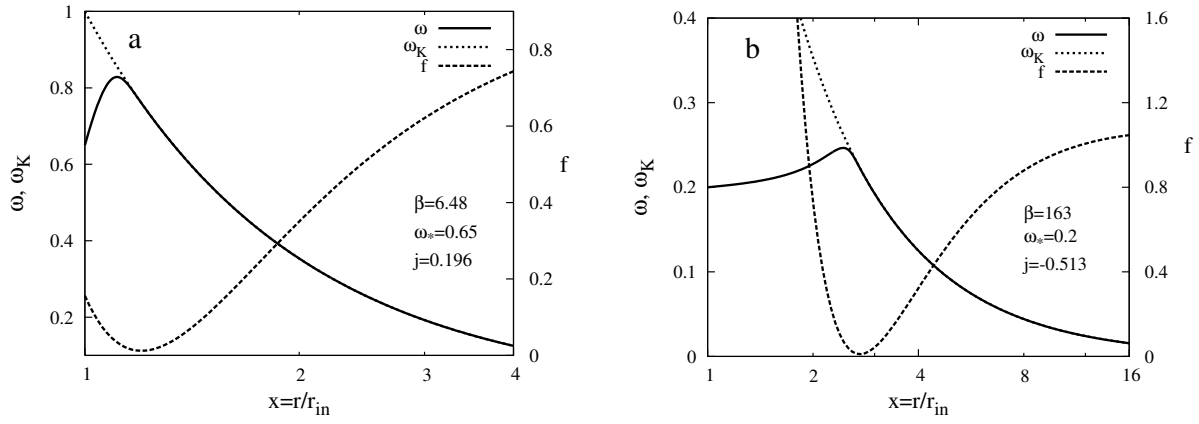


Fig. 3.— Estimated rotation rate profiles $\omega(x) \equiv \Omega/\Omega_K(r_{\text{in}})$ and the corresponding normalized vertically integrated dynamical viscosities $f(x) = 3\pi\nu\Sigma/\dot{M}$ for a magnetically threaded disk around an X-ray pulsar with observed parameters appropriate for 4U 1626 – 67 before and after the torque reversal. The panel (a) represents the angular velocity transition zone during the spin-up episode. The transition region is broad as seen from panel (b) when the source is in spin-down state. The rotation rate profiles $\omega(x)$ shown by *solid curves* in panels (a) and (b) obtain for $\beta = 6.48$, $\omega_* = 0.65$, $j \simeq 0.196$ and $\beta = 163$, $\omega_* = 0.2$, $j \simeq -0.513$, respectively. In each panel the *dashed curve* corresponds to $f(x)$ and the *dotted curve* to the Keplerian profile $\omega_K(x) = x^{-3/2}$, where $x \equiv r/r_{\text{in}}$.

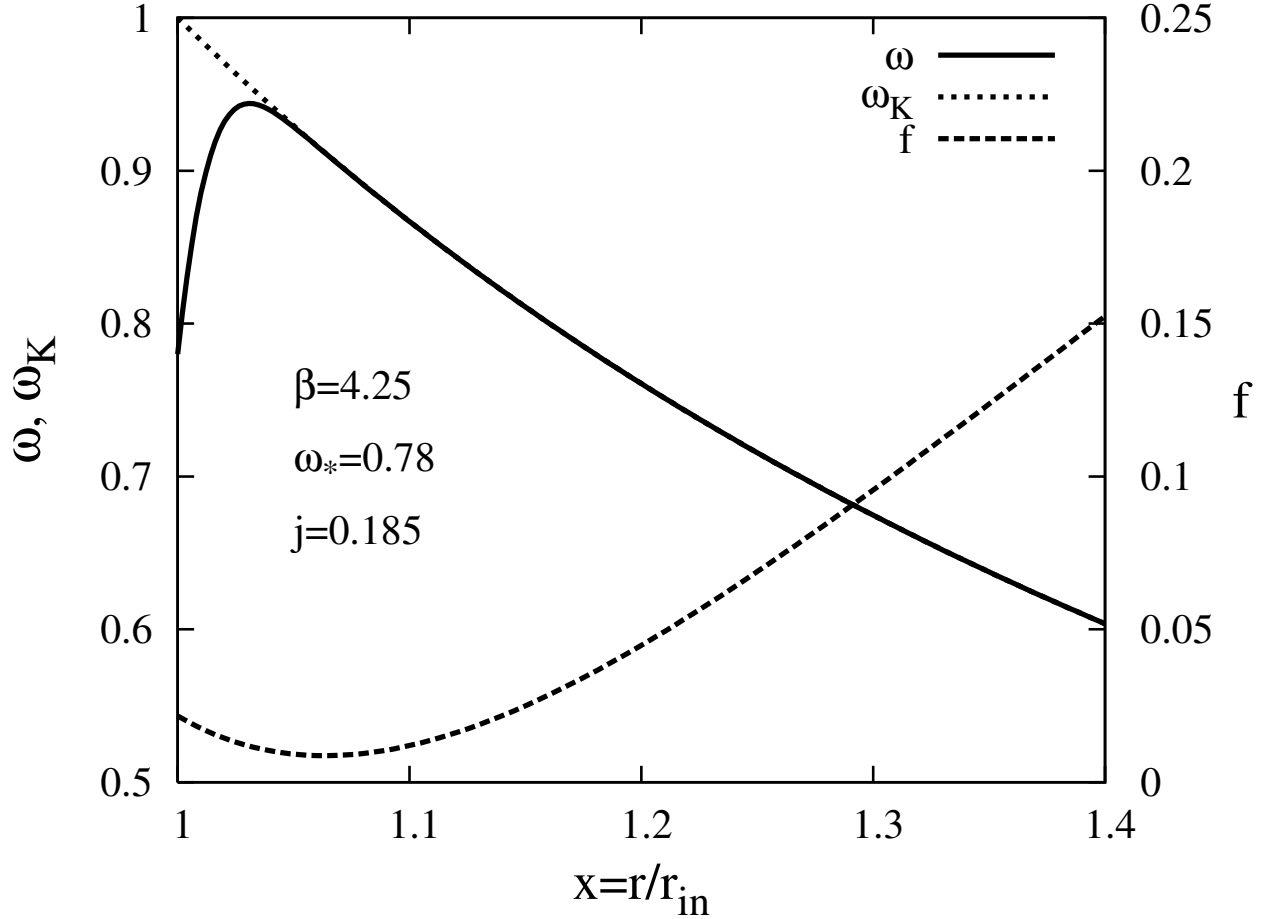


Fig. 4.— Radial variation of angular velocity $\omega(x) \equiv \Omega/\Omega_K(r_{\text{in}})$ and the corresponding normalized vertically integrated dynamical viscosity $f(x) = 3\pi\nu\Sigma/\dot{M}$ for a disk around an X-ray pulsar with observed parameters appropriate for 4U 0115 + 63. The rotation rate profile $\omega(x)$ shown by the *solid curve* obtains for $\beta = 4.25$, $\omega_* = 0.78$, $j \simeq 0.185$. The *dashed curve* corresponds to $f(x)$ and the *dotted curve* to the Keplerian profile $\omega_K(x) = x^{-3/2}$, where $x \equiv r/r_{\text{in}}$.

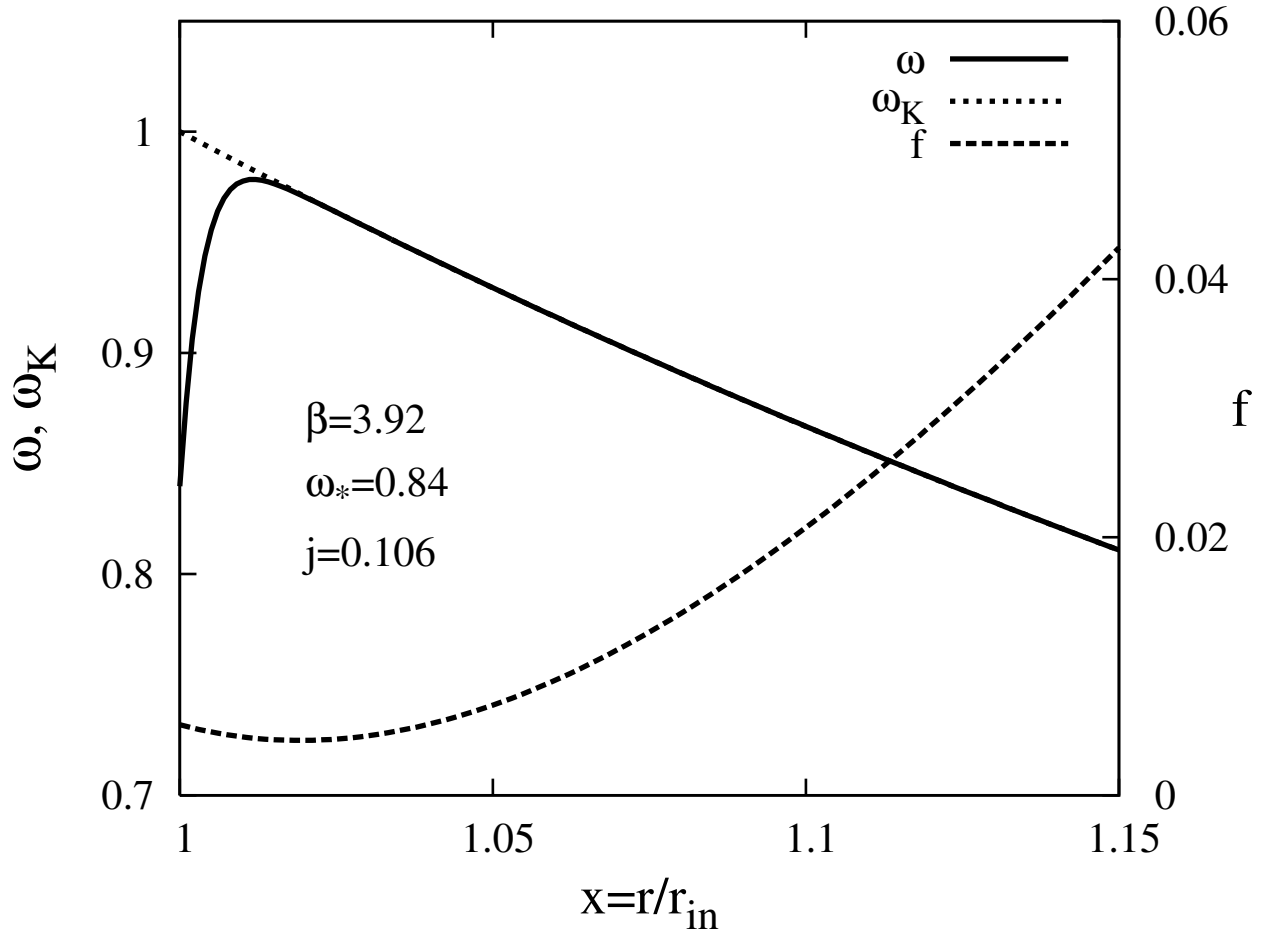


Fig. 5.— Radial variation of angular velocity $\omega(x) \equiv \Omega/\Omega_K(r_{\text{in}})$ and the corresponding normalized vertically integrated dynamical viscosity $f(x) = 3\pi\nu\Sigma/\dot{M}$ for a disk around an X-ray pulsar with observed parameters appropriate for Cen X-3. The rotation rate profile $\omega(x)$ shown by the *solid curve* obtains for $\beta = 3.92$, $\omega_* = 0.84$, $j \simeq 0.106$. The *dashed curve* corresponds to $f(x)$ and the *dotted curve* to the Keplerian profile $\omega_K(x) = x^{-3/2}$, where $x \equiv r/r_{\text{in}}$.